Draft version March 21, 2018
Typeset using LaTeX **twocolumn** style in AASTeX61

CORE COSMOLOGY LIBRARY: PRECISION COSMOLOGICAL PREDICTIONS FOR LSST

Husni Almoubayyed,[1] David Alonso,[2] Jonathan Blazek,[3,4] Philip Bull,[5,6] Jean-Éric Campagne,[7] N. Elisa Chisari,[2] Alex Drlica-Wagner,[8] Zilong Du,[9] Tim Eifler,[10,11] John Ellison,[9] Renée Hlozek,[12] Mustapha Ishak,[13] Matthew Kirby,[14] David Kirkby,[15] Elisabeth Krause,[16] C. Danielle Leonard,[1] Christiane S. Lorenz,[2] Phil Marshall,[17] Thomas McClintock,[14] Sean McLaughlin,[18] Jérémy Neveu,[7] Stéphane Plaszczynski,[7] Javier Sanchez,[15] Sukhdeep Singh,[1,19] Anže Slosar,[20] Antonio Villarreal,[21] Michal Vrastil,[22] and Joe Zuntz[23]
(LSST Dark Energy Science Collaboration)

[1] *McWilliams Center for Cosmology, Department of Physics, Carnegie Mellon University, Pittsburgh, PA 15213, USA*
[2] *Department of Physics, University of Oxford, Denys Wilkinson building, Keble Road, Oxford OX1 3RH, United Kingdom*
[3] *Center for Cosmology and Astroparticle Physics, Ohio State, Columbus, OH 43210, USA*
[4] *Laboratory of Astrophysics, École Polytechnique Fédérale de Lausanne (EPFL), Observatoire de Sauverny, 1290 Versoix, Switzerland*
[5] *Department of Astronomy, University of California Berkeley, Berkeley, CA 94720, USA*
[6] *Radio Astronomy Laboratory, University of California Berkeley, Berkeley, CA 94720, USA*
[7] *Laboratoire de l'Accélérateur Linéaire, Université Paris-Sud, CNRS/IN2P3, Université Paris-Saclay, Orsay, France*
[8] *Fermi National Accelerator Laboratory, P. O. Box 500, Batavia, IL 60510, USA*
[9] *Department of Physics and Astronomy, University of California, Riverside, CA 92521, USA*
[10] *Jet Propulsion Laboratory, California Institute of Technology, Pasadena, CA 91109, USA*
[11] *Department of Physics, California Institute of Technology, Pasadena, CA 91125, USA*
[12] *Dunlap Institute for Astronomy and Astrophysics & Department for Astronomy and Astrophysics, University of Toronto, ON M5S 3H4*
[13] *Department of Physics, The University of Texas at Dallas, Richardson, TX 75083, USA*
[14] *Univeristy of Arizona, Tucson, AZ 85721, USA*
[15] *Department of Physics and Astronomy, University of California, Irvine, CA 92697, USA*
[16] *Kavli Institute for Particle Astrophysics and Cosmology, Stanford, CA 94305-4085, USA*
[17] *SLAC National Accelerator Laboratory, Menlo Park, CA 94025, USA*
[18] *Stanford University, Stanford, CA, 94305, USA*
[19] *Berkeley Center for Cosmological Physics and Department of Physics, University of California, Berkeley, California*
[20] *Brookhaven National Laboratory, Physics Department, Upton, NY 11973, USA*
[21] *Department of Physics and Astronomy, University of Pittsburgh, Pittsburgh PA 15260*
[22] *Institute of Physics CAS, Prague, 182 21, CZ*
[23] *Institute for Astronomy, Royal Observatory Edinburgh, Edinburgh EH9 3HJ, UK*

ABSTRACT

The Core Cosmology Library (`CCL`) provides routines to compute basic cosmological observables with validated numerical accuracy. These routines have been validated to an accuracy level, documented here, against the results of the Code Comparison Project. In the current version, predictions are provided for distances and background quantities, angular auto- and cross-spectra of cosmic shear and clustering, and the halo mass function. Fiducial specifications for the expected LSST galaxy distributions and clustering bias are also included, together with the capability of computing redshift distributions for a user-defined photometric redshift model. `CCL` is written in C, with a Python interface.

Contents

1. INTRODUCTION

Volunteer(s) in charge: Mustapha Ishak

Tentative: An era of precision cosmology is at the door with the advent of a number of high precision surveys. One of them is the Large Synoptic Survey Telescope (LSST) that is designed to address the question of cosmic acceleration and the Dark Energy associated with it.

In preparation for constraining cosmology with LSST, it is necessary to be able to produce rigorous (and accurate?) theoretical predictions for the cosmological quantities that will be measured. The Core Cosmology Library[1] (`CCL`) aims to provide, in one library, a way of making predictions that are validated to a well-documented numerical accuracy, for the purpose of constraining cosmology with LSST. By constructing a cosmology library specifically with LSST and its Dark Energy Science Collaboration (DESC) in mind, it is possible to ensure that it is flexible, adaptable, and validated for all cases of interest, as well as user-friendly and appropriate for the needs of all DESC working groups.

`CCL` computes basic cosmological functions including the Hubble parameter, distances, density parameters, and linear growth functions. It calculates the matter power spectrum using various methods including common approximations, calls to external software such as `CLASS` (Blas et al. 2011), or emulators such as the "Cosmic Emulator" of Lawrence et al. (2017). It computes 2-point angular power spectra and correlation functions from various probes, going beyond the Limber approximation. `CCL`'s overall structure is illustrated in figure DA:missing figure.

`CCL`'s implementation includes spatially flat and curved Λ-Cold Dark Matter (ΛCDM) cosmologies, and wCDM cosmologies with the option of using a time-dependent equation of state. It also allows the use of massive neutrinos. (is Table 1 up to date?).

Finally, it is worth noting that while `CCL` is built in light of LSST, its flexible and modular structure is designed to work with any other pipelines and surveys.

To do: Summarize the probes we cover. Explain future link to likelihood pipeline. Highlight CCL can be used by other surveys.

2. COSMOLOGICAL MODELS AND OBSERVABLES

Volunteer(s) in charge: Renee

The overarching goal of `CCL` is to allow seamless integration of different cosmological models of interest to

[1] https://github.com/LSSTDESC/CCL

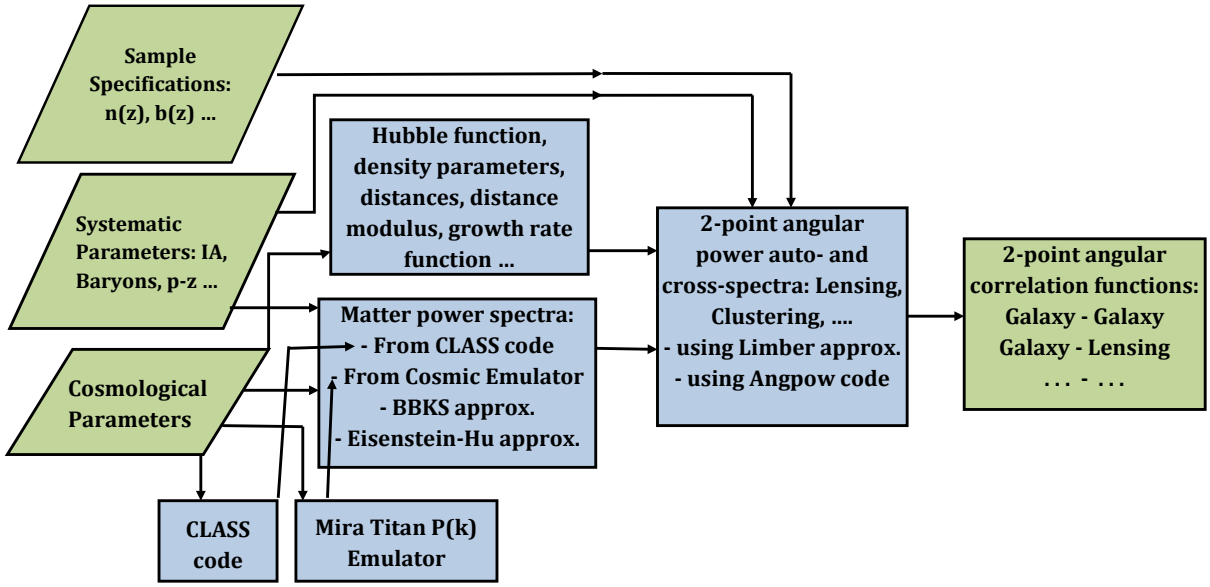

Figure 1. CCL structure flowchart. CCL is written in C with a Python interface. CCL routines calculate basic cosmological functions such as Hubble function, density parameters, distances and growth function. It uses various methods to compute the matter-power spectrum including CLASS, "Cosmic Emulator" developed by Lawrence et al. (2017), or common approximations. It computes 2-point angular power spectra and correlation functions from various probes. CCL is designed to accommodate multiple methods to calculate cosmological observables.

LSST, given some priors on the range of validity of the specific models.

The cosmological components include the matter density parameter Ω_m, the dark energy density Ω_Λ, the radiation density Ω_r, the curvature density Ω_K, the neutrino density of both massless and massive neutrinos, given by $\Omega_{\nu,\mathrm{rel}}$ and $\Omega_{\nu,\mathrm{m}}$ respectively, the optical depth τ, and parameters for the equation of state of dark energy.

Currently, the following families of models are supported:

- Flat ΛCDM cosmology with parameters Ω_b, n_s, A_s or σ_8, Ω_m, Ω_Λ, τ and a cosmological constant dark energy model with equation-of-state $w = -1$.

- wCDM and the Chevallier-Polarski-Linder (CPL) model for dark energy and it's redshift dependence ($w(a) = w_0 + w_a(1-a)$, Chevallier & Polarski 2001 and Linder 2003)

- A universe with non-zero curvature (K) so that the curvature energy density (density parameter (MI)) is the difference of sum of the energy densities of the other components with respect to unity (flatness), i.e. $\Omega_k = 1 - \sum_i \Omega_i$.

- All of the above, plus an arbitrary, user-defined modified growth function (see description in Section 2.2).

- Massive neutrino species in combination with any of the above except the user-defined modified growth function, specified by either Σm_ν (which maps on to the density $\Omega_{\nu,\mathrm{m}}$ above), or by the individual masses of each of three neutrino species.

In the particular case of cosmologies with massive neutrinos, CCL allows the user to specify either a sum of masses, Σm_ν, or the individual mass of each of three neutrino species. In the former case, CCL will by default split Σm_ν into three neutrino masses which are consistent with the normal hierarchy (see, e.g. Lattanzi & Gerbino (2017) for a review). However, the user can alternatively ask for Σm_ν to be split either into masses consistent with the inverted hierarchy, or into equal masses. Each mass is then checked for whether it is non-relativistic (massive) at $z = 0$, and this information is used in combination with the user-provided value of N_{eff} (the effective number of relativistic neutrino species in the early universe) to set the number of relativistic neutrino species.

Not all features of CCL are available for all models. For a guide to which predictions are available for each model, see Table 1. Note that if users install their own version of CLASS, CCL can then make predictions for a more extended set of cosmologies. Users should take care to understand the validity of the CCL assumptions for their own models.

Table 1. Cosmologies implemented in CCL.

Observable/Model	flat ΛCDM	ΛCDM+K	ΛCDM + m_ν	wCDM	$w_0 + w_a$	MG
Distances	✓	✓	✓	✓	✓	X
Growth	✓	✓	X	✓	✓	✓
$P_m(k, z)$	✓	✓	✓	✓	✓	X
Halo Mass Function	✓	✓	X	✓	✓	X
C_l, number counts	✓	✓	X	✓	✓	X
C_l, weak lensing only	✓	✓	✓	✓	✓	X
Correlation function	✓	✓	✓	✓	✓	X

2.1. *Background cosmology*

Volunteer(s) in charge: Renee

Suggested content: Background cosmology parameter definition. Expansion and distance functions. Growth function and growth rate. The models that are specified above map directly onto cosmological observables like the expansion rate of the universe, which is paramterised through the Hubble parameter (and assuming the CPL parameterization described above) as:

$$\frac{H(a)}{H_0} = a^{-3/2}\Big(\Omega_{M,0} + \Omega_{\Lambda,0}a^{-3(w_0+w_a)}\exp[3w_a(a-1)]+ \Omega_{K,0}a + (\Omega_{g,0}+\Omega_{\nu,\mathrm{rel}})a^{-1} + \Omega_{\nu,\mathrm{m}}(a)a^3\Big)^{\frac{1}{2}}. \quad (1)$$

where $\Omega_{\nu,\mathrm{m}}(a)$, the fractional energy density of massive neutrinos, is calculated via

$$\Omega_{\nu,\mathrm{m}}(a) = \sum_{i=1}^{N_\nu} \frac{8\pi^2(\pi k_b)^3 k_b}{15(ch_\mathrm{P})^3}\frac{8\pi G}{3h^2c^2}\left(\frac{T_\nu^{\mathrm{eff}}}{a}\right)^4 \times \left(\frac{7}{8}\int_0^{x_{\max}} dx\, x^2 \frac{\sqrt{x^2+(\mu^i)^2}}{\exp(x)+1}\right). \quad (2)$$

Here, h_P is Planck's constant, h is $H_0/100$ with H_0 in units of km / s / Mpc, and T_ν^{eff} is the effective temperature of massive neutrinos. T_ν^{eff} is related to the temperature of the CMB via $T_\nu^{\mathrm{eff}} = T_{\mathrm{CMB}}T_{\mathrm{NCDM}}$, where T_{NCDM} is a dimensionless factor used by e.g. `CLASS` to set the ratio of $\frac{\sum m_\nu}{\Omega_\nu^0}$ to its experimentally measured value. Note that T_{NCDM} is used to modulate the effective temperatuer of massive neutrinos only; the temperature of relativistic neutrinos follows the usual relation. Finally, μ^i is a per-species, mass-like dimensionless value, given by $\mu^i = m_\nu^i a/T_\nu^{\mathrm{eff}}$.

In order to compute distances, we use the radial comoving distance, which is calculated via a numerical integral as

$$\chi(a) = c\int_a^1 \frac{da'}{a'^2 H(a')}. \quad (3)$$

The transverse comoving distance is then computed in terms of the radial comoving distance as:

$$r(\chi) = \begin{cases} k^{-1/2}\sin(k^{1/2}\chi) & k>0 \\ \chi & k=0 \\ |k|^{-1/2}\sinh(|k|^{1/2}\chi) & k<0 \end{cases} \quad (4)$$

This function can be written directly in terms of the energy density in cosmic curvature, Ω_k, as:

$$r(\chi) = \frac{c}{H_0}\sqrt{\Omega_k}\sinh(\sqrt{\Omega_k}\chi), \quad (5)$$

which is valid for all forms of the curvature energy density.

The angular diameter distance is $d_A = a\,r(a)$, and the luminosity distance is $d_L = r(a)/a$, leading to the familiar relation $d_A = a^2 d_L$ which is valid in general for all metric theories of gravity.

The `CCL` suite also has the functionality to compute the distance modulus, defined as,

$$\mu = 5\log_{10}(d_L/\mathrm{pc}) - 5 \quad (6)$$

and $a(\chi)$, the inverse of $\chi(a)$.

2.2. *Growth of perturbations*

Volunteer(s) in charge: Mustapha Ishak

To compute the linear growth factor of matter perturbations, $D(a)$, `CCL` solves the following usual differential equation:

$$\frac{d}{da}\left(a^3 H(a)\frac{dD}{da}\right) = \frac{3}{2}\Omega_M(a)aH(a)D, \quad (7)$$

using a Runge-Kutta Cash-Karp algorithm.

In doing this, `CCL` simultaneously computes the logarithmic growth rate $f(a)$, defined as:

$$f(a) = \frac{d\ln D}{d\ln a}. \quad (8)$$

CCL provides different functions that return the growth normalized to $D(a=1)=1$ and to $D(a\ll 1)\to a$. It employs an accelerated spline that is linearly spaced in the scale factor to interpolate the growth functions.

The growth calculations cover flat and curved ΛCDM, wCDM, and (w_0+w_a)CDM cosmologies. However, it should be noted that the above treatment is strictly valid for a Universe containing only dust-like matter components. A scale-independent growth rate is, for example, ill-defined in the presence of massive neutrinos which are not included in CCL's growth calculation.

Finally, CCL allows for an alternative 'modified gravity' cosmological model defined by a regular background (w_0+w_a)CDM (To do: with arbitrary K?) as well as a user-defined $\Delta f(a)$, such that the true growth rate in this model is given by $f(a)=f_0(a)+\Delta f(a)$, where $f_0(a)$ is the growth rate in the background model. Note that this model is only consistently implemented with regards to the computation of the linear growth factor and growth rates (which will also scale the linear power spectrum). All other CCL functions (including the non-linear power spectrum) will ignore these modifications. This model, and the interpretation of the predictions given by CCL, should therefore be used with care.To do: What is the mapping between $\Delta f(a)$ and MG theories?

2.3. *Matter power spectrum*

Volunteer(s) in charge: Elisa Chisari

Suggested content: Matter power spectrum and transfer function definition. Approximations. Cosmic emulator. Baryonic physics model.

Theoretical predictions for cosmological observables such as galaxy clustering, gravitational lensing and cluster mass functions rely on knowledge of the distribution of matter from small to large scales in the Universe. The quantity most frequently used to describe the distribution of matter at a given wavenumber and redshift is the matter power spectrum, $P(k,z)$, defined as

$$\langle\tilde{\delta}(\mathbf{k},z)\tilde{\delta}(\mathbf{k}',z)\rangle=(2\pi)^3P(k,z)\;\delta_D^3(\mathbf{k}-\mathbf{k}') \qquad (9)$$

where $\tilde{\delta}(\mathbf{k})$ is the Fourier component of the overdensity field at a given wavenumber and δ_D^3 is the Dirac delta function. $P(k,z)$ has units of volume and a dimensionless analogue is often defined as

$$\Delta^2(k,z)\equiv\frac{k^3}{2\pi^2}P(k,z). \qquad (10)$$

CCL implements several different methods for making predictions for the matter power spectrum. Two of those methods, the BBKS (Bardeen et al. 1986) and Eisenstein & Hu (1998) approximations are only accurate to within a few percent and are implemented for validation purposes only. These approximations provide analytical expressions for the transfer function, $T(k)$, which is related to the matter power spectrum by $\Delta(k)^2\propto T^2(k)k^{3+n_s}$, where n_s. The normalization of the power spectrum is defined at $z=0$ by setting σ_8 to its value today.

The default CCL implementation uses the CLASS algorithm Blas et al. (2011) to obtain predictions for $P(k,z)$. In addition, CCL can also generate $P(k,z)$ predictions by emulation of cosmological numerical simuations, in particular, using the "Cosmic Emulator" developed by Lawrence et al. (2017).

None of the previous methods account for the impact of baryonic physics on the distribution of matter, which is known to exceed percent level at scales $k\gtrsim 1/\mathrm{Mpc}$ (van Daalen et al. 2011; Vogelsberger et al. 2014; Hellwing et al. 2016; Springel et al. 2017) and can affect the extraction of cosmological parameters (Semboloni et al. 2011, 2013; Mohammed & Seljak 2014; Eifler et al. 2015; Mohammed & Gnedin 2017). To account for this effect, we incorporate in CCL an effective parametrisation (Schneider & Teyssier 2015) of the redistribution of matter as a consequence of feedback from Active Galactic Nuclei and adiabatic cooling. This parametrisation reproduces results from the OWLS (van Daalen et al. 2011) simulations at $z=0$. We give an overview of each method in what follows.

BBKS approximation. CCL implements the analytical BBKS approximation to the transfer function (Bardeen et al. 1986), given by

$$T\;(q\equiv k/\Gamma h\mathrm{Mpc}^{-1})=\frac{\ln[1+2.34q]}{2.34q}\times \qquad (11)$$
$$[1+3.89q+(16.2q)^2+(5.47q)^3+(6.71q)^4]^{-0.25}$$

where $\Gamma=\Omega_m h$. The BBKS power spectrum option is primarily used as a precisely-defined input for testing the numerical accuracy of CCL routines (as described in Sec. DA:missing section),and it is not recommended for other uses.

Eisenstein & Hu approximation. CCL also provides an approximation to the matter power spectrum as implemented by Eisenstein & Hu (1998) (we refer the reader to this paper for a detailed discussion of the fitting formulae).[2]

CLASS. The default configuration of CCL adopts predictions for the nonlinear matter power spectrum from this publicly available software (Blas et al. 2011). CLASS

[2] Note that the implementation in CCL modifies Eq. 5 of Eisenstein & Hu (1998) using $a^{-1}=1+z$ instead of the approximation $a^{-1}\sim z$. The difference in the resulting power spectra is negligible, but larger than 1 part in 10^4 for $k<10\,h\,\mathrm{Mpc}^{-1}$.

currently computes the non-linear power spectrum using the HaloFit prescription of Takahashi et al. (2012).

Cosmic emulator. The emulator (Lawrence et al. 2017) provides accurate predictions for the nonlinear matter power spectrum, at the 1% level for $z \leq 2$ and in the wavenumber range $k = [10^{-3}, 5]$ Mpc^{-1}. The allowed range of cosmological parameters that can be passed to the emulator is as follows:

$$\begin{aligned} 0.12 \leq \Omega_m h^2 &\leq 0.155, \\ 0.0215 \leq \Omega_b h^2 &\leq 0.0235, \\ 0.7 \leq \sigma_8 &\leq 0.9, \\ 0.55 \leq h &\leq 0.85, \\ 0.85 \leq n_s &\leq 1.05, \\ -1.3 \leq w_0 &\leq -0.7, \\ -1.73 \leq w_a &\leq -0.7,^{3} \\ 0.0 \leq \Omega_\nu h^2 &\leq 0.01.^{4} \end{aligned} \tag{12}$$

Baryonic correction model (BCM). CCL incorporates the impact of baryons on the total matter power spectrum via the BCM of Schneider & Teyssier (2015). The main consequences of baryonic processes are: to suppress the power spectrum at intermediate scales ($k \sim$ a few h/Mpc) due to the ejection of gas by Active Galactic Nuclei feedback, and to enhance it at smaller scales due to adiabatic cooling. To account for these effects, BCM uses an effective decomposition for the impact of gas ejection (G) and the enhancement of the small scale profile due to star formation (S) to estimate the fractional effect of baryonic processes on the dark matter-only power spectrum ($P_{\rm DMO}$):

$$P_{\rm BCM}(k,z) = P_{\rm DMO}(k,z) G(k|M_c, \eta_b, z) S(k|k_s) \tag{13}$$

Three effective parameters govern the contribution of baryonic processes to modifying the total matter power spectrum:

- $\log_{10}[M_c/(\mathrm{M}_\odot/h)]$: the mass of the clusters responsible for feedback, which regulates the amount of suppression of the matter power spectrum at intermediate scales;
- η_b: a dimensionless parameter which determines the scale at which suppression peaks;
- and k_s [h/Mpc]: the wavenumber that determines the scale of the stellar profile.

If these parameters are not specified by the user, CCL assumes the default parameters of Schneider & Teyssier (2015), which are in agreement with results from OWLS.

2.4. *2-point correlators*

Volunteer(s) in charge: David Alonso, Tom McClintock

Suggested content: Kernels. Correlation functions. Nuisance parameters and functions.

In this section we will distinguish between *tracers* (quantities observed on the sky, such as number counts in a redshift bin, shear, or CMB temperature fluctuations) and *contributions* to the total observed fluctuations of these tracers (such as the biased matter density term in number counts, redshift-space distortions, magnification, etc.).

2.4.1. *Angular power spectra*

The angular power spectrum between two tracers a and b can be written as:

$$C_\ell^{ab} = 4\pi \int_0^\infty \frac{dk}{k} \mathcal{P}_\Phi(k) \Delta_\ell^a(k) \Delta_\ell^b(k), \tag{14}$$

where $\mathcal{P}_\Phi(k)$ is the dimensionless power spectrum of the primordial curvature perturbations, and Δ^a and Δ^b are the transfer functions corresponding to these tracers. Each transfer function will receive contributions from different terms. Currently CCL supports three types of tracers: number counts, galaxy shape distortions and lensing convergence, with the following contributions:

Number counts.—The transfer function for number counts can be decomposed into three contributions: $\Delta^{\rm NC} = \Delta^{\rm D} + \Delta^{\rm RSD} + \Delta^{\rm M}$, where

- $\Delta^{\rm D}$ is the standard density term proportional to the matter density:

$$\Delta_\ell^{\rm D}(k) = \int dz\, p_z(z)\, b(z)\, T_\delta(k,z)\, j_\ell(k\chi(z)), \tag{15}$$

  where $j_\ell(x)$ is ℓ-th order spherical Bessel function, T_δ is the matter transfer function, $b(z)$ is the linear clustering bias for this tracer and $p_z(z)$ is the normalized distribution of sources in redshift (i.e. the selection function). The fluctuations in the number density of sources in different redshift bins are therefore treated by CCL as different tracers. Note that CCL currently does not support non-linear or scale-dependent bias, but future releases of it will do so under a number of schemes, including perturbative approaches as implemented in e.g. McEwen et al. (2016a).

- $\Delta^{\rm RSD}$ is the linear contribution from redshift-space distortions:

$$\Delta_\ell^{\rm RSD}(k) = \int dz\, \frac{(1+z) p_z(z)}{H(z)} T_\theta(k,z) j_\ell''(k\chi(z)), \tag{16}$$

where $T_\theta(k,z)$ is the transfer function of θ, the divergence of the comoving velocity field. Note that the RSD contribution to number counts is currently computed by `CCL` assuming a linear-theory relation between the matter overdensity and peculiar velocity fields, mediated by the scale-independent growth rate f. While this should not be problematic for wide photometric redshift bins and standard cosmological models, users should exercise care when interpreting results for narrow window functions or exotic cosmologies.

- $\Delta^{\rm M}$ is the contribution from lensing magnification:

$$\Delta^{\rm M}_\ell(k) = -\ell(\ell+1)\int \frac{dz}{H(z)} W^{\rm M}(z) T_{\phi+\psi}(k,z) j_\ell(k\chi(z)), \quad (17)$$

where $T_{\phi+\psi}$ is the transfer function for the Newtonian-gauge scalar metric perturbations, and $W^{\rm M}$ is the magnification window function:

$$W^{\rm M}(z) \equiv \int_z^\infty dz'\, p_z(z') \frac{2-5s(z')}{2} \frac{r(\chi'-\chi)}{r(\chi')r(\chi)}. \quad (18)$$

To do: Is it not $r(chi') - r(\chi)$ normally at numerator ? same for other integrals below. (from Jeremy, comparing with Bonvin et al. and other references) Here $s(z)$ is the magnification bias, given as the logarithmic derivative of the number of sources with magnitude limit, and $r(\chi)$ is the angular comoving distance (see Eq. 4).

Note that `CCL` currently does not compute relativistic corrections to number counts Challinor & Lewis (2011); Bonvin & Durrer (2011). Although these will be included in the future, their contribution to the total fluctuation is largely subdominant (see Alonso et al. (2015) and the two references above), and therefore it is safe to work without them in most cases.

Correlated galaxy shapes.—The transfer function for correlated galaxy shapes (intrinsic and lensed) is currently decomposed into two terms: $\Delta^{\rm SH} = \Delta^{\rm WL} + \Delta^{\rm IA}$, where

- $\Delta^{\rm L}$ is the standard lensing ("cosmic shear") contribution:

$$\Delta^{\rm L}_\ell(k) = -\frac{1}{2}\sqrt{\frac{(\ell+2)!}{(\ell-2)!}} \int \frac{dz}{H(z)} W^{\rm L}(z) T_{\phi+\psi}(k,z) j_\ell(k\chi(z)), \quad (19)$$

where $W^{\rm L}$ is the lensing kernel, given by

$$W^{L}(z) \equiv \int_z^\infty dz' p_z(z') \frac{r(\chi'-\chi)}{r(\chi')r(\chi)}. \quad (20)$$

- $\Delta^{\rm IA}$ is the transfer function for intrinsic galaxy alignments. `CCL` currently supports the so-called "non-linear alignment model", in which the intrinsic galaxy inertia tensor is proportional the local tidal tensor Hirata & Seljak (2004); Hirata et al. (2007):

$$\Delta^{\rm IA}_\ell(k) = \sqrt{\frac{(\ell+2)!}{(\ell-2)!}} \int dz\, p_z(z)\, b_{\rm IA}(z)\, f_{\rm red}(z)\, T_\delta(k,z) \frac{j_\ell(k\chi(z))}{(k\chi(z))^2}. \quad (21)$$

Here $b_{\rm IA}$ is the so-called alignment bias, and $f_{\rm red}$ is the fraction of red galaxies in the sample. It is understood that only red galaxies are subject to this type of alignment mechanism. Suggested content: Elisa, check if phrasing is correct?

Lensing convergence.—The transfer function for the lensing convergence of a given source plane at redshift z_* receives only one contribution, given by

$$\Delta^{\kappa}_\ell(k) = -\frac{\ell(\ell+1)}{2}\int_0^{\chi_*} \frac{dz}{H(z)} \frac{r(\chi_*-\chi)}{r(\chi)r(\chi_*)} T_{\phi+\psi}(k,z), \quad (22)$$

where $\chi_* \equiv \chi(z_*)$.

It is worth noting that the equations above should be modified for non-flat cosmologies by replacing the spherical Bessel functions j_ℓ with their hyperspherical counterparts Kamionkowski & Spergel (1994). These are currently not supported by `CCL`, and their impact is mostly relevant on low multipoles. This will be revisited in future versions of the library.

2.4.2. *Correlation functions*

Volunteer(s) in charge: Elisa Chisari, Sukhdeep Singh? The following expressions relating the angular power spectra and correlation functions are valid in the flat-sky approximation[5]. In all cases, $f_K(\chi)$ is comoving angular diameter distance, which differs from the radial comoving distance χ only in the case of cosmologies with non-zero curvature.

Galaxy-galaxy. The angular correlation function between two number-count tracers (labeled a and b here) is given by

$$\xi^{ab}(\theta) = \int d\ell \frac{\ell}{2\pi} C^{ab}_\ell J_0(\ell\theta), \quad (23)$$

where C_{ab} is the angular power spectrum between both tracers.

[5] See the weak lensing review by Bartelmann & Schneider (2001), page 44 and Joachimi & Bridle (2010).

Lensing-lensing. The lensing correlation functions are [6]

$$\xi^{ab}_{+}(\theta) = \int_0^\infty d\ell \frac{\ell}{2\pi} J_0(\ell\theta) C^{ab}_\ell, \tag{24}$$

$$\xi^{ab}_{-}(\theta) = \int_0^\infty d\ell \frac{\ell}{2\pi} J_4(\ell\theta) C^{ab}_\ell, \tag{25}$$

where the angular lensing convergence power spectrum C^{ab}_ℓ is given above (see Equations 19 and 42).

Galaxy-lensing. The correlation between a number count tracer a and a shear tracer b is given by

$$\xi^{ab}(\theta) = \int d\ell \frac{\ell}{2\pi} C^{ab}_\ell \, J_2(\ell\theta), \tag{26}$$

3-dimensional spatial correlation function.

In addition to the angular correlation functions, the 3-dimensional spatial correlation function $\xi(r)$ is calculated from the power spectrum $P(k)$ using

$$\xi(r) = \frac{1}{2\pi^2} \int dk \, k^2 P(k) \frac{\sin(kr)}{kr} \tag{27}$$

2.5. *Halo mass function*

Volunteer(s) in charge: Antonio Villarreal - Could Use Review

Volunteer(s) in charge: Tom - made edits. Text written by Antonio that I changed is left as comments. Remove when ready. Removed discussion of bias from this section.

Being able to calculate the halo abundance as a function of mass is a necessary step to being able to constrain cosmology with probes such as galaxy clustering. While analytic functions are the traditional means of predicting evolution, calibration is frequently required against cosmological simulations. In order to reach the high precision for cosmological constraints in a self-consistent fashion, it is ultimately necessary to use cosmological simulations; we implement this with halo mass functions with parameters fit to these simulations. The calculation of the halo mass function focuses around the spherical overdensity method of halo finding, in which the size of a halo can be defined with:

$$\bar{\rho}(r_\Delta) = \Delta \times \bar{\rho}_{\rm m}, \tag{28}$$

where a spherical halo with radius r_Δ has an average density $\bar{\rho}$ equal to the overdensity parameter Δ times the mean background density of the universe, $\rho_{\rm m}$. Within the literature, the choice of Δ can vary considerably, as observations focusing on the compact cores of haloes often take much larger values of Δ, while the fiducial definition in most halo clustering studies is a definition of $\Delta = 200$. We note that another common definition exists which utilizes the critical density of the universe, $\rho_{\rm crit}$; this introduces a simple conversion factor between the two definitions that must be accounted for. Currently, `CCL` only accepts overdensity parameters with respect to the mean matter density, but we plan to allow for self-consistent handling of critical density based definitions in the future.

The halo mass function is defined as

$$\frac{dn}{dM} = f(\sigma) \frac{\bar{\rho}_{\rm m}}{M} \frac{d \ln \sigma^{-1}}{dM}, \tag{29}$$

where n is the number density of halos of a given mass M associated with the RMS variance of the matter density field σ^2. In CCL calling this function returns the mass function in logarithmic mass bins, $dn/d\log_{10} M$, where the input is the halo mass M and scale factor a.

The halo mass M is related to σ by first computing the radius R that would enclose a mass M in a homogeneous Universe at $z = 0$:

$$M = \frac{H_0^2}{2G} R^3 \rightarrow \frac{M}{M_\odot} = 1.162 \times 10^{12} \Omega_M h^2 \left(\frac{R}{1\,{\rm Mpc}} \right)^3. \tag{30}$$

The RMS density contrast in spheres of radius R can then be computed as

$$\sigma_R^2 = \frac{1}{2\pi^2} \int dk \, k^2 \, P(k) \, \tilde{W}_R^2(k) \tag{31}$$

where $P(k)$ is the linear matter power spectrum and $\tilde{W}(kR)$ is the Fourier transform of a spherical top hat window function,

$$\tilde{W}_R(k) = \frac{3}{(kR)^3} [\sin(kR) - kR\cos(kR)]. \tag{32}$$

One commonly used halo mass function definition within the literature is the Tinker et al. (2010) fitting function. This fitting function has been developed using collisionless N-body simulation data, using haloes determined by spherical overdensities. This is an extension of the Tinker et al. (2008) halo mass function, which is also included within `CCL` as a comparative option. This fitting function assumes little change with respect to cosmological parameters. Further, it includes a redshift scaling with is assumed to sharply end at a redshift of $z = 3$. This halo mass function is calibrated within the range of $10^{10.5} h{\rm M}_\odot \leq M \leq 10^{15.5} h{\rm M}_\odot$ at a redshift of $z = 0$.

For purposes of comparison, we also have included the results of Angulo et al. (2012), which uses the Millenium

[6] from Schneider 2002 and Bartelmann & Schneider section 6.4.1

XXL simulation in order to study galaxy cluster scaling relations. As part of this study, they have calculated their own fit to the Tinker et al. (2010) fitting function. While this additional halo mass function is available, it has not been extended to a broad range of overdensity parameter Δ, nor has it been extended beyond a redshift of $z = 0$.

The Tinker et al. (2008) fitting function uses the following parameterisation for the multiplicity function:

$$f(\sigma) = A\left[\left(\frac{\sigma}{b}\right)^{-a} + 1\right]e^{-c/\sigma^2}, \tag{33}$$

where A, a, b, and c are fitting parameters that have additional redshift scaling and σ is the RMS variance of the density field smoothed on some scale M at some scale factor a. This basic form is modified for the Angulo et al. (2012) formulation. The resulting form is

$$f(\sigma) = A\left[\left(\frac{b}{\sigma} + 1\right)^{-a}\right]e^{-c/\sigma^2}, \tag{34}$$

where the only change is in the formulation of the second term. Note that the fitting parameters in the Angulo et al. (2012) formulation do not contain any redshift dependence and the use of it is primarily for testing and benchmark purposes.

The Tinker et al. (2010) model parameterizes the halo mass function in terms of the peak height, $\nu = \delta_c/\sigma(M)$, where $\delta_c = 1.686$ is the critical density for collapse. The multiplicity function is then written as

$$f(\nu) = \alpha[1 + (\beta\nu)^{-2\phi}]\nu^{2\eta}e(-\gamma\nu^2/2). \tag{35}$$

We note that these halo mass functions, while implemented to high *numerical* accuracy, carry their own uncertainties. It has not been significantly studied whether the halo mass function (or halo bias function) is universal with respect to changes in dark energy parameterisation. Tinker et al. (2008, 2010) quote 5% accuracy of their mass funcitons. This result is consistent with the work of Watson et al. (2013), which also finds a 5% level difference in comparison to the Tinker fitting function. Further study will be required in the future in order to gain percent level accuracy in determining the halo mass function.

2.6. *Halo bias*

Volunteer(s) in charge: Antonio Villarreal
Suggested content: Halo bias definition.

An important step in many interpretations of the halo model is to have a measure of the bias of dark matter halos, defined as the ratio of the halo power spectrum to the linear dark matter power spectrum,

$$b^2(k) = \frac{P_h(k)}{P_{\rm lin}(k)}. \tag{36}$$

As with measures of the halo mass function, high accuracy cosmological constraints requires the use of numerical simulations to develop fitting functions and emulators. We note that we will define haloes as in the above subsection focusing on the halo mass function. `CCL` currently implements the halo bias fitting function results in Tinker et al. (2010), though future improvements will likely require the use of emulator methods.

The Tinker et al. (2010) model parameterizes the halo bias in terms of the peak height, $\nu = \delta_c/\sigma(M)$, where δ_c is the critical density for collapse and is chosen to be 1.686 for this particular parameterization. We can then parameterize the halo function and halo bias as

$$b(\nu) = 1 - A\frac{\nu^a}{\nu^a + {\delta_c}^a} + B\nu^b + C\nu^c, \tag{37}$$

$$f(\nu) = \alpha[1 + (\beta\nu)^{-2\phi}]\nu^{2\eta}e(-\gamma\nu^2/2). \tag{38}$$

Again, while high *numerical* accuracy has been verified, there is a remaining uncertainty. Tinker et al. (2010) found a $\sim 6\%$ scatter when determining the halo bias due to differences in simulations alone. In addition, this parameterization does not include a careful exploration of any impact due to changes in the dark energy equation of state. As with the halo mass function, studies will be required to reach accuracy at the percent level for any cosmological predictions.

3. IMPLEMENTATION OF HIGH-ACCURACY COSMOLOGICAL FUNCTIONS

3.1. *Background functions & growth of perturbations*

Volunteer(s) in charge: Mustapha Ishak Suggested content: Initial conditions. Normalization. Units and sensitivity to physical constants (G, c etc).

Including/excluding radiation in the computation of the comoving distances and the growth function can easily make a difference of 10^{-4} at the redshifts required in this comparison.

We have performed a comparison of the physical constants used in `CCL` to those used in `GSL` and `CLASS` as well as published sources such as the NIST Handbook and PDG Review of Particle Physics To do: The comparison was with PDG2013, we could update that.. Where possible, we have set constants to the values that are used internally in `CLASS`. This includes the value of the gravitational constant, the Boltzmann constant, the Planck constant, the speed of light, and the electron charge. `CLASS` does not include a definition of the solar mass or the Stefan-Boltzmann constant so we use the values used by `GSL`. After comparison between the physical constants used in `CCL` and those of the sources mentioned above, we have found better than 10^{-4} agreement with everything except the gravitational constant.

The value of the gravitational constant, G, enters into the critical density. We found that failure to define G with sufficient precision would result in lack of convergence at the 10^{-4} level between the different submissions. Importantly, note that CAMB barely has 10^{-4} precision in G (and similarly, there might be other constants within CAMB/CLASS for which one should check the precision level). For `CCL`, we are using the value from `CLASS`.

3.2. *Matter power spectrum*

Volunteer(s) in charge: Elisa Chisari

Suggested content: Interpolation strategy. Sensitivity to spline parameters and sampling in k. Settings that control speed vs. accuracy.

For the matter power spectrum, the spline is performed in two variables: the logarithmically-spaced wavenumber and the logarithmically and linearly-spaced scale factor. Splining the `CLASS` output leads to some precision loss (compared to direct outputs from `CLASS`). We quantify this, along with the impact of extrapolation, in the following subsection.

The computation of the power spectrum from `CLASS` can be significantly sped up by extrapolating in the range $k >$ `K_MAX_SPLINE` and $k <$ `K_MIN`. In this section, we describe the implementation of the extrapolation and the accuracy attained. These tests are performed in a flat ΛCDM cosmology with $\Omega_c = 0.25$, $\Omega_b = 0.05$, $A_s = 2.1 \times 10^{-9}$, $h = 0.7$ and $n_s = 0.96$.

We first describe the extrapolation at high wavenumbers. The introduction of the parameter `K_MAX_SPLINE` allows us to spline the matter power spectrum within the `cosmo` structure up to that value of k (in units of 1/Mpc). A separate `K_MAX` parameter sets the limit for evaluation of the matter power spectrum. The range between `K_MAX_SPLINE` $< k <$ `K_MAX` is evaluated by performing a second order Taylor expansion in $\ln k$ within the static routine `ccl_power_extrapol_highk`.

First, we compute the first and second derivative of $\ln P(k, z)$ at $k_0 =$ `K_MAX` $- 2\Delta \ln k$ by computing the numerical derivatives by finite differences using GSL. The fiducial choice for $\Delta \ln k$ is 10^{-2}. We then apply a second order Taylor expansion to extrapolate the matter power spectrum to $k >$ `K_MAX_SPLINE`. The Taylor expansion gives

$$\ln P(k,z) \simeq \ln P(k_0,z) + \frac{d\ln P}{d\ln k}(\ln k_0, z)(\ln k - \ln k_0) + \frac{1}{2}\frac{d^2 \ln P}{d\ln k^2}(\ln k_0, z)(\ln k - \ln k_0)^2. \quad (39)$$

The accuracy of this approximation is shown in Figure 2 for redshifts $z = 0$, $z = 3$ and $z = 20$. We compare the nonlinear matter power spectrum at these redshifts, computed with the previously described approximation, to the matter power spectrum obtained by setting the power spectrum splines to high values. We find that for typical values of $\Delta \ln k = 10^{-2}$ and `K_MAX_SPLINE`$= 50$/Mpc, $\ln P$ has converged to an accuracy that surpasses the expected impact of baryonic effects on the matter power spectrum at $k > 10$/Mpc. (For an estimate of the impact of baryons on the total matter power spectrum, see Schneider & Teyssier 2015.) The lower `K_MAX_SPLINE` is, the faster `CCL` will run. The optimum choice of `K_MAX_SPLINE` is left to the user for their particular application.

We also extrapolate the power spectrum at small wavenumbers within the static routine `ccl_power_extrapol_lowk`. In this case, the power spectrum below `K_MIN` is obtained by a power-law extrapolation with index n_s:

$$\log P(k < \texttt{K\_MIN}, z) = \log P(\texttt{K\_MIN}, z) + n_s(\log k - \log \texttt{K\_MIN}) \quad (40)$$

The value adopted for `K_MIN` depends on the choice of power spectrum method. For CLASS and the nonlinear power spectrum, we adopt `K_MIN` that coincides with the smallest wavenumber output by CLASS, `K_MIN`$= 7 \times 10^{-6}$/Mpc.[7] Note that this parameter is different from `K_MIN_DEFAULT`, which sets the minimum k for integrations and which is set by default to `K_MIN_DEFAULT`$= 5 \times 10^{-5}$/Mpc. Hence, in practice, no extrapolation is occurring in this case, unless the user specifically asks for an output power spectra below `K_MIN_DEFAULT` for their own purposes.

With the implementation described above, the power spectrum splines are initialized up to `K_MAX_SPLINE`. This is also true for the linear matter power spectrum, which is used within `CCL` in particular to obtain σ_8 (see Eq. 31). We have tested how the procedure described in the previous section affects the convergence of the linear matter power spectrum. We compare the fiducial `CCL` output to the case where we set `K_MAX_SPLINE` $= 5 \times 10^3$/Mpc. The result is shown in Figure 2. For some applications that use the linear power spectrum, the user might need to increase the value of `K_MAX_SPLINE`.

As in the previous section, the power spectrum at small wavenumber is extrapolated using a power-law. This extrapolation is performed below a fiducial value of `K_MIN_DEFAULT`$= 5 \times 10^{-5}$.

[7] For BBKS, the power spectrum is computed analytically at all k, there is no extrapolation. For the Eisenstein & Hu implementation, the splines of the power spectrum span `K_MIN_DEFAULT`$< k <$`K_MAX_SPLINE`, so there is only extrapolation at high k.

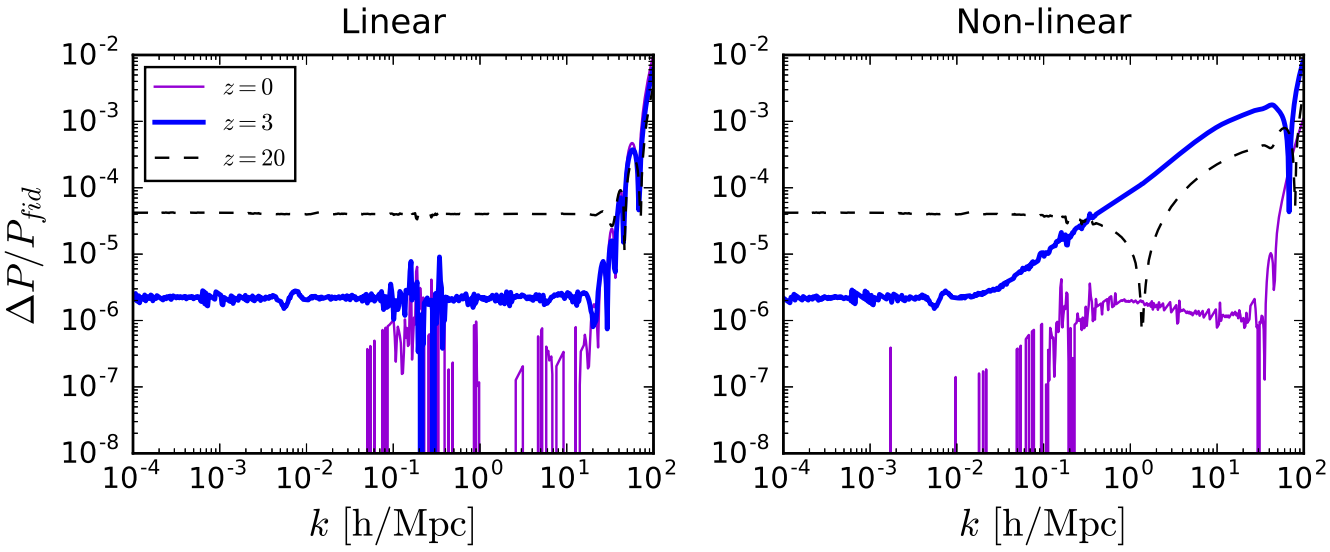

Figure 2. The relative error compared to power spectra produced with high values of the power spectrum splines, P_{fid}, produced by splining the matter power spectrum up to `K_MAX_SPLINE` and extrapolating beyond this value with a second order Taylor expansion the natural logarithm of the matter power spectrum. The left panel shows the relative errors for the linear matter power spectrum at $z = 0$, $z = 3$ and $z = 20$. The right panel shows the results for the non-linear matter power spectrum at the same redshifts. The standard `CCL` parameters adopted are those corresponding to the black dashed curve. For comparison, the impact of baryonic physics on the matter power spectrum is $\sim 10\%$ at $k = 1$/Mpc (Schneider & Teyssier 2015).

We have found that changing `A_SPLINE_NA_PK` to 200, or changing `N_K` to 5000, does not change the results presented in Figures 2 in this section.

3.3. *Angular power spectra*

Volunteer(s) in charge: David Alonso

Different numerical approaches have been implemented in the library in order to expedite the computation of angular power spectra. We describe these here.

3.3.1. *Limber approximation*

Volunteer(s) in charge: David Alonso, Jérémy Neveu

As shown in Section 2.4.1, computing each transfer function contributing to a given power spectrum involves a radial projection (i.e. an integral over redshift or z or χ), and thus computing full power spectra consists of a triple integral for each ℓ. This can be computationally intensive, but can be significantly simplified in certain regimes by using the Limber approximation, given by:

$$j_\ell(x) \simeq \sqrt{\frac{\pi}{2\ell+1}}\,\delta\left(\ell+\frac{1}{2}-x\right). \tag{41}$$

Thus for each k and ℓ we can define a radial distance $\chi_\ell \equiv (\ell+1/2)/k$, with corresponding redshift z_ℓ. This approximation works best for wide radial kernels and high multipoles.

Substituting this in the expressions above, the simplified versions become:

$$C_\ell^{ab} = \frac{2}{2\ell+1}\int_0^\infty dk\, P_\delta\,(k, z_\ell)\,\tilde{\Delta}_\ell^a(k)\tilde{\Delta}_\ell^b(k). \tag{42}$$

where

$$\tilde{\Delta}_\ell^{\rm D}(k) = p_z(z_\ell)\, b(z_\ell)\, H(z_\ell) \tag{43}$$

$$\tilde{\Delta}_\ell^{\rm RSD}(k) = \frac{1+8\ell}{(2\ell+1)^2}\, p_z(z_\ell)\, f(z_\ell)\, H(z_\ell) - \tag{44}$$

$$\frac{4}{2\ell+3}\sqrt{\frac{2\ell+1}{2\ell+3}} p_z(z_{\ell+1})\, f(z_{\ell+1})\, H(z_{\ell+1}) \tag{45}$$

$$\tilde{\Delta}_\ell^{\rm M}(k) = 3\Omega_{M,0}H_0^2\frac{\ell(\ell+1)}{k^2}\,\frac{(1+z_\ell)}{\chi_\ell}W^{\rm M}(z_\ell) \tag{46}$$

$$\tilde{\Delta}_\ell^{\rm L}(k) = \frac{3}{2}\Omega_{M,0}H_0^2\sqrt{\frac{(\ell+2)!}{(\ell-2)}}\,\frac{1}{k^2}\,\frac{1+z_\ell}{\chi_\ell}W^{\rm L}(z_\ell) \tag{47}$$

$$\tilde{\Delta}_\ell^{\rm IA}(k) = \sqrt{\frac{(\ell+2)!}{(\ell-2)!}}\frac{p_z(z_\ell)\, b_{\rm IA}(z_\ell) f_{\rm red}(z_\ell) H(z_\ell)}{(\ell+1/2)^2} \tag{48}$$

3.3.2. *Beyond Limber:* `Angpow`

Volunteer(s) in charge: Jérémy Neveu

`CCL` incorporates natively routines to compute the C_ℓ^{ab} angular power spectra as described above without the Limber approximation. The algorithm performs first the integrals over z for both tracers, and ends with the k integral. This computation is much slower than using the

Limber approximation, but it ends up with precise angular power spectra at low ℓ, and correct cross-correlations between tracers (the Limber approximation fails at reproducing the beat phenomenon $j_\ell(x) \times j_\ell(x')$). The integration of these routines has been tested against the `CLASS` code and recover the same angular power spectra when precision parameters are set to high values.

However, the computation of the C_ℓ^{ab} without the Limber approximation is too costly in terms of computing time using this method, if one wants to explore extensively a full cosmological parameter space. The aim of the `Angpow` software (Campagne et al. 2017) is to compute the angular power spectra C_ℓ^{ab} without any Limber numerical approximation in a faster way but still accurately. `CCL` has been linked to the `Angpow` code, which is briefly described here.

The angular power spectrum for two tracers C_ℓ^{ab} is computed in `Angpow` according to the following expression

$$C_\ell^{ab} = \iint_0^\infty \mathrm{d}z\mathrm{d}z' p_{z_1}(z_1) p_{z_2}(z') \times \int_0^\infty \mathrm{d}k\, f_\ell(z,k) f_\ell(z',k). \tag{49}$$

The auxiliary function $f_\ell(z,k)$ can be defined without loss of generality as

$$f_\ell(z,k) \equiv \sqrt{\frac{2}{\pi}}\, k\sqrt{P_\delta(k,z)}\, \widetilde{\Delta}_\ell(z,k) \tag{50}$$

with $\widetilde{\Delta}_\ell(z,k)$ the function describing the physical processes such as matter density fluctuations, redshift-space distortions as described for instance in references Durrer (2008); Yoo et al. (2009); Yoo (2010); Challinor & Lewis (2011); Bonvin & Durrer (2011). Currently, the `Angpow` version delivered with `CCL` only can deal with galaxy clustering tracers (no lensing) and this without the magnification lensing term (equation 17). The incorporation of those transfer functions is left for a future work, but in principle `Angpow` has already the capability to treat them. For now, for galaxy clustering tracers we define $\widetilde{\Delta}_\ell(z,k)$ as

$$\widetilde{\Delta}_\ell(z,k) \approx b(z) j_\ell(k\chi(z)) - f(z) j_\ell''(k\chi(z)) \tag{51}$$

with $j_\ell(x)$ and $j_\ell''(x)$ the spherical Bessel function of order ℓ and its second derivative, and $f(z)$ the growth rate of structures.

In `Angpow`, the inner integral in k is computed first. To conduct the computation of such integral of highly oscillating functions, the 3C-algorithm described in details in reference (Campagne et al. 2017) is used. In brief, it lies on the projection of the oscillating $f_\ell(z,k)$ onto Chebyshev series of order 2^N, the product of the two Chebyshev series is performed with a 2^{2N} Chebyshev serie; then, the integral is computed thanks to a Clenshaw-Curtis quadrature. At the end the integrals over z are performed via again an optimised Clenshaw-Curtis quadrature. All the Chebyshev expansions and the Clenshaw-Curtis quadrature are performed via the *Discrete Cosine Transform* of type I from the DCT-I fast transform of FFTW library.

The `Angpow` software was tested against `CLASS` and the native `CCL` computation and can perform the same computations approximately an order of magnitude faster ($\mathcal{O}(1s)$). Its precision and speed parameters are optimised so that the relative numerical error compared with an high precision computation is two orders of magnitude below the relative cosmic variance $\sqrt{2/(2\ell+1)}$, from $\ell = 2$ to $\ell = 1000$.

As in the general case the Limber approximation is valid at high ℓ values, the `CCL` user can define an ℓ threshold to switch from the non-Limber slow computation to the faster Limber approximation.

3.4. *Correlation functions*

Volunteer(s) in charge: Elisa Chisari, Sukhdeep Singh?

Suggested content: Which basis to work in. Approach to performing oscillatory integrals.

In this section we describe the computation of correlation functions given the angular power spectrum.

We begin by briefly deriving the relation between correlation functions and power spectra. A (scalar) angular space observable, X, with spin s can be decompsed into spin spherical harmonics

$$X(\vec{\Omega}) = \sum_{\ell m} \tilde{X}_{\ell m}\ {}_sY_{\ell m}(\vec{\Omega}) \tag{52}$$

where $\vec{\Omega}$ refers to the angular coordinates on the sky. The angular cross correlation function of two tracers, X and Z of the large scale structure can be written in terms of their harmonic components, $\tilde{X}_{\ell m}$ and $\tilde{Z}_{\ell' m'}$ as

$$\langle XZ\rangle(\theta) = \left\langle \sum_{\ell,m}\sum_{\ell',m'} \tilde{X}_{\ell m}\tilde{Z}_{\ell' m'}\ {}_{s_X}Y_{\ell m}(\vec{\Omega})\ {}_{s_Z}Y_{\ell' m'}(\vec{\Omega}+\theta) \right\rangle \tag{53}$$

$$= \sum_{\ell,m} C_\ell\ {}_{s_X}Y_{\ell m}(\vec{\Omega})\ {}_{s_Z}Y_{\ell m}(\vec{\Omega}+\theta) \tag{54}$$

where s_X and s_Z are the spins of tracers, ${}_sY_{\ell m}$ are spin spherical harmonics and we also used the identity

$$\langle \tilde{X}_{\ell m}\tilde{Z}_{\ell' m'}\rangle = C_\ell \delta_D(m,m')\delta_D(\ell,\ell'), \tag{55}$$

Using the addition theorem for spin spherical harmonics and the relation between spherical harmonics and wigner

D-matrices[8] (Ng & Liu 1999), we can write

$$\langle XZ\rangle(\theta) = \frac{1}{4\pi}\sum_\ell (2\ell+1) C_\ell D^\ell_{s_X,-s_Z}(0,\theta,0) \quad (56)$$

The galaxy number count is spin zero and shear is a spin-2 object. Thus the expressions for various auto and cross correlations are To do: expand to full width of page

$$\xi_{gg}(\theta) = \frac{1}{4\pi}\sum_\ell (2\ell+1) C^{gg}_\ell D^\ell_{0,0}(0,\theta,0) = \frac{1}{4\pi}\sum_\ell (2\ell+1) C^{gg}_\ell P_\ell(\cos\theta) \quad (57)$$

$$\langle g\gamma_T\rangle(\theta) = \frac{1}{4\pi}\sum_\ell (2\ell+1) C^{g\gamma}_\ell D^\ell_{2,0}(0,\theta,0) = \frac{1}{4\pi}\sum_\ell (2\ell+1)\sqrt{\frac{(\ell-2)!}{(\ell+2)!}} C^{g\gamma}_\ell P^2_\ell(\cos\theta) \quad (58)$$

$$\langle g\kappa\rangle(\theta) = \frac{1}{4\pi}\sum_\ell (2\ell+1) C^{g\kappa}_\ell D^\ell_{0,0}(0,\theta,0) = \frac{1}{4\pi}\sum_\ell (2\ell+1) C^{g\kappa}_\ell P_\ell(\cos\theta) \quad (59)$$

$$\xi_+(\theta) = \frac{1}{4\pi}\sum_\ell (2\ell+1) C^{\gamma\gamma *}_\ell D^\ell_{2,2}(0,\theta,0) \quad (60)$$

$$\xi_-(\theta) = \frac{1}{4\pi}\sum_\ell (2\ell+1) C^{\gamma\gamma *}_\ell D^\ell_{2,-2}(0,\theta,0) \quad (61)$$

Using relations from Kilbinger et al. (2017), we can write

$$C^{g\kappa}_\ell = \frac{1}{2}\frac{(\ell+1)!}{(\ell-1)!} C^{g\psi}_\ell \quad (62)$$

$$C^{g\gamma}_\ell = \frac{1}{2}\sqrt{\frac{(\ell+2)!}{(\ell-2)!}} C^{g\psi}_\ell \quad (63)$$

$$\langle g\gamma_T\rangle(\theta) = \frac{1}{4\pi}\sum_\ell \frac{(2\ell+1)}{\ell(\ell+1)} C^{g\kappa}_\ell P^2_\ell(\cos\theta)\,. \quad (64)$$

The `ccl_tracer_corr_legendre` routine computes these transform to convert angular power spectra, C_ℓ, into correlation functions. We use the associated Legendre function implementation from the `GSL` library. `ccl_tracer_corr_legendre` routine evaluations can be very slow, especially for polynomials P^m_ℓ with $m > 0$. Note that the P^m_ℓ evaluations need to be done only once and can then be saved as long as ℓ and θ values do not change. However, `CCL` has not yet implemented this feature.

The `ccl_tracer_corr_legendre` methods currently does not support the computation of the shear correlation functions $\xi_\pm$, and the approximate `ccl_tracer_corr_fftlog` (described below) should be used instead. As demonstrated in Kilbinger et al. (2017) and Kitching et al. (2017), this approximation should be sufficient even for futuristic surveys.

Hankel Transform—Notice that in the flat-sky limit, the expressions in Eqs. 57–61 can be written as Hankel transforms using the relation between $D^\ell_{m,m'}$ and the Bessel functions J (for $\ell \gg m, m'$)

$$D^l_{m,m'}(0,\theta,0) \approx J_{m-m'}(\ell\theta) \quad (65)$$

The same expressions can also be derived from Eqs. 60–61 using the relation between P^m_ℓ and the Bessel functions J_m (de Putter & Takada 2010)

$$P^m_\ell(\cos\theta) = (-1)^m \frac{(\ell+m)!}{(\ell-m)!}\ell^{-m} J_m(\ell\theta) \quad (66)$$

which yields final expressions that coincide with Eq. 25. For numerical integration to get (projected) correlation functions using Hankel transform, we make use of the public code `FFTlog`[9] (Hamilton 2000; Talman 2009). In brief, `FFTlog` works on functions periodic in log space, by writing the Hankel Transform as a convolution between Bessel functions and the function of interest (in this case C_ℓ). A version of this code is included in `CCL` with minor modifications.

3.5. *Halo mass function*

Volunteer(s) in charge: Antonio Villarreal - Could Use Review

Suggested content: Evaluation of derivatives. Interpolations for different values of Δ. Precision of $\sigma(M)$ calculation.

To achieve 10^{-4} precision in $\sigma(M)$ and the normalisation of the power spectrum, one should check that the integral of σ_8 and $\sigma(M)$ has converged for the chosen values of $\{k_{\rm min}, k_{\rm max}\}$. After checking convergence, we achieved the desired precision.

Also note that for $\sigma(M)$, it is important to set the desired precision level correctly for the numerical integrator. The integral usually yields $\sigma^2(M)$, and not $\sigma(M)$. Hence, one has to set the desired precision taking the exponent into account.

Derivatives are calculated utilizing a spline that is built off of the previously described $\sigma(M)$ spline. As such, these splines cover the range from 10^6 to $10^{17} M_\odot$. For each value of $\log(M)$ in our spline evaluation, we calculate the value of $\sigma(M)$ half a step in either direction. We use the difference compared to the mass spacing to calculate an approximate derivative, which is then used in the spline interpolation. This has been tested to meet

[8] https://en.wikipedia.org/wiki/Wigner_D-matrix

[9] http://casa.colorado.edu/~ajsh/FFTLog/

our necessary precision for the halo mass function within the mass range explored by Tinker et al. (2010). We note that there the accuracy is reduced at the edges of these splines and exploring extreme mass ranges may require changes in the parameters to initialize these splines.

In order to accomodate a wide range of values of the overdensity parameter Δ, we have generated a spline interpolation between best fit values as defined by Tinker et al. (2008) and Tinker et al. (2010). This covers a dynamic range from $\Delta = 200$ to 3200. Within this range, we interpolate in the space of the fit parameter and $\log \Delta$ using the Akima interpolation built from piecewise third order polynomials. We have chosen this rather than the fitting formulas utilized in Tinker et al. (2010) in order to assure high precision match to the Tinker halo mass function when choosing a value of *Delta* directly from the paper.

3.6. *Massive neutrinos*

Volunteer(s) in charge: Danielle Leonard

Suggested content: Approximations. Approach to performing integrals.

3.7. *Implementation of photometric redshifts*

Volunteer(s) in charge: Danielle Leonard

Suggested content: Explain approach to photometric redshifts and flexibility to pass user-defined function.

Redshifts of LSST galaxies will be obtained via photometry. Therefore, performing any cosmological analysis which incorporates redshift information therefore requires a model for the probability of measuring a photometric redshift $z_{\rm ph}$ for an object with hypothetical spectroscopic redshift $z_{\rm s}$. In order to maintain agnosticism towards the optimal model, and hence to allow for the future inclusion of advancements from ongoing research, `CCL` allows the user to flexibly input a photometric redshift model. In addition, for ease of use, `CCL` provides the option of using a built-in function for a simple Gaussian photometric redshift probability distribution.

In order to use `CCL` with a custom-input photometric redshift model, the user writes a function which accepts as input a photometric redshift, a spectroscopic redshift, and a pointer to a structure containing any further parameters of the model. This function will return the probability of measuring the input photometric redshift given the input spectroscopic redshift. The photometric redshift model can then be used, for example, when computing $\frac{dN}{dz}^i$ in photometric redshift bin i, as given by:

$$\frac{dN}{dz}^i = \frac{\frac{dN}{dz}\int_{z_i}^{z_{i+1}} dz' p(z,z')}{\int_{z_{\rm min}}^{z_{\rm max}} dz \frac{dN}{dz}\int_{z_i}^{z_{i+1}} dz' p(z,z')} \qquad (67)$$

where $p(z,z')$ is the photometric redshift probability distribution, and z_i and z_{i+1} are the photo-z edges of the bin in question. In the case of the simple Gaussian photometric redshift model for which support is included in `CCL` out of the box, $p(z,z')$ is given as

$$p(z,z') = \frac{1}{\sqrt{2\pi}\sigma_z}\exp\left(-\frac{(z-z')^2}{2\sigma_z^2}\right). \qquad (68)$$

4. VALIDATION OVER THE ΛCDM PARAMETER SPACE

4.1. *Accuracy criteria*

Volunteer(s) in charge: ?

Suggested content: Why we chose the 10^{-4} level of accuracy. Accuracy summary statistic used in VARRIC.

4.2. *Validation tests on fiducial parameter sets*

Volunteer(s) in charge: Elisa Chisari, Antonio Villarreal, Phil Bull, Elisabeth Krause

Suggested content: Overview of the code comparison. How the codes used for comparison were selected. Validation plots for several observables.

Our goal is for outputs of `CCL` to be validated against the results of a code-comparison project run within LSST-DESC down to a 10^{-4} or pre-established accuracy level if possible. In some cases, this level of accuracy is not necessary, as other systematics which have not yet been considered in this version of `CCL` are expected to have a larger fractional impact. In the cases where this applies, we make it clear below.

A code comparison project was carried out among members of TJP where the following outputs of cosmological forecast codes were compared and validated:

1. growth factor at $z = 0, 1, 2, 3, 4, 5$,
2. comoving radial distance [Mpc/h] at the same redshifts, as well as the corresponding distance moduli,
3. linear matter power spectrum, $P(k)$, from BBKS (Bardeen et al. 1986) in units of $({\rm Mpc}/h)^3$ at $z = 0, 2$ in the range $10^{-3} \leq k \leq 10h/{\rm Mpc}$ with 10 bins per decade,
4. Eisenstein & Hu matter power spectrum in units of $({\rm Mpc}/h)^3$ at $z = 0$ in the range $10^{-3} \leq k \leq 10h/{\rm Mpc}$ with 10 bins per decade, and
5. the mass variance at $z = 0$, $\sigma(M, z = 0)$ for $M = \{10^6, 10^8, 10^{10}, 10^{12}, 10^{14}, 10^{16}\}{\rm M}_\odot/h$.

These predictions were produced and compared for different cosmologies, which are listed in the table below. The results agree to better than 0.1% relative accuracy

Cosmological models for code comparison project								
Model	Ω_m	Ω_b	Ω_Λ	h_0	σ_8	n_s	w_0	w_a
flat LCDM	0.3	0.05	0.7	0.7	0.8	0.96	-1	0
w_0 LCDM	0.3	0.05	0.7	0.7	0.8	0.96	-0.9	0
w_a LCDM	0.3	0.05	0.7	0.7	0.8	0.96	-0.9	0.1
open w_a LCDM	0.3	0.05	0.65	0.7	0.8	0.96	-0.9	0.1
closed w_a LCDM	0.3	0.05	0.75	0.7	0.8	0.96	-0.9	0.1

Table 2. Cosmological models for code comparison project.

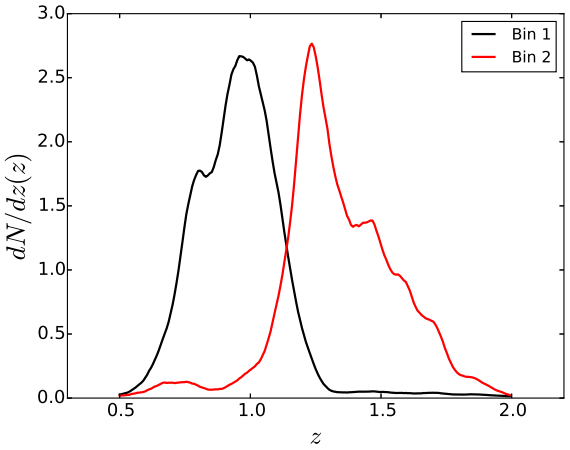

Figure 3. Binned redshift distributions used for code comparison project.

for comoving distance and growth factor among all submissions, and for $P(k)$ and $\sigma(M)$ among codes which use the same BBKS conventions.

We noticed that there are 2 typographical errors for the BBKS transfer function in "Modern Cosmology" (Dodelson 2004) compared to the original BBKS paper. The quadratic term should be $(16.1q)^2$ and the cubic term should be $(5.46q)^3$. The BBKS equation is correct in Peacock (1999). Using the wrong equation can give differences in the results above the 10^{-4} level.

In a second stage, we used the BBKS linear matter power spectrum from the previous step to compare two-point statistics for two redshift bins, resulting in three tomography combinations, $(1-1)$,$(1-2)$,$(2-2)$. We computed the following quantities:

- projected galaxy clustering tomography power spectra: density term only (no magnification, RSD, etc.) with non-evolving linear bias $b(z) = 1$, in the range $10 < \ell < 10000$, using 5 bins per decade,
- angular convergence tomography power spectra: leading order convergence term only (no magnification), in the same range and with the same resolution as the case above,
- angular galaxy clustering tomography correlation function, in the range $0.01\,\mathrm{deg} < \theta < 5\,\mathrm{deg}$, using 5 bins per decade, and
- angular shear tomography correlation functions (ξ_+,ξ_-), similarly to above.

We adopted the following analytic redshift distributions: a Gaussian with $\sigma = 0.15$, centered at $z_1 = 1$; and another Gaussian with the same dispersion but centered at $z_2 = 1.5$. We repeated the exercise for two redshift distribution histograms shown in Figure 3.

In this second step, only 2 codes have been compared so far. More outputs are needed to guarantee convergence. From these outputs, we have concluded that:

- The cross-correlation between bins is particularly sensitive to the number of points where the kernels have been sampled.
- The accuracy of the correlation function is sensitive to $\ell_{\rm max}$. We had to use up to $\ell_{\rm max} = 3 \times 10^4$ for convergence (and we could not achieve 0.01% convergence).
- The large scales of the correlation function are sensitive to $\ell_{\rm min}$. The use of the flat-sky approximation is also relevant on these scales.
- For sufficiently high precision, the correlation functions are sensitive to how the power spectrum is sampled and interpolated.

For C_ℓ computations, we required the relative difference between `CCL` and the benchmarks to be $< 10^{-3}$. We performed the test both for analytic redshift distributions and histograms.

To obtain realistic targets for the convergence of correlation function computations for LSST analyses, we calculate the expected statistical uncertainty of the clustering and lensing correlation functions of the LSST gold sample (c.f. Sect. DA:missing section),assuming an effective source galaxy density of $n_{\rm eff} = 26\mathrm{gal/sq\,arcmin}$ for galaxy shape distortions, and galaxy density of $n_{\rm gold} = 45\mathrm{gal/sq\,arcmin}$ for number counts. Specifically, we calculate the Gaussian covariance of angular correlation functions following the formalism of Joachimi et al. (2008), and note that leaving out the non-Gaussian covariance terms makes this convergence criterion more conservative. We split the galaxy samples into 10 tomography bins, defined to contain equal numbers of galaxies. The accuracy test then proceeds as follows. We

compared the difference between CCL calculated lensing and clustering correlations and the benchmarks for the analytic redshift distributions and for auto-correlations of redshift bins only. To pass the benchmark test, we required that this difference be smaller than half of the value of the errorbar derived from the covariance for each correlation function computed. Specifically, we take the value of the covariance in the bins centered at $z = 1$ and $z = 1.5$ to compare to the benchmarks.

The 3-dimensional correlation function $\xi(r)$ was validated by comparing with an independent transform code based on the method of Ogata (2005) implemented in the hankel.py python package. We calculate $\xi(r)$ by transforming the CCL BBKS linear power spectrum using this independent code and using a fine sampling of $P(k)$. This is done for the five cosmologies listed in Table 2 and redshifts $z = 0, 1, 2, 3, 4, 5$. We then compare with the $\xi(r)$ from CCL with a sampling of $P(k)$ equal to N_K_3DCOR bins per decade. The default value of N_K_3DCOR $= 1000$ results in fractional agreement at the level of $< 4 \times 10^{-3}$ for $0.1 < r < 50$ Mpc increasing to < 0.01 at $r = 100$ Mpc. Above this scale $\xi(r)$ approaches zero. If higher accuracy is desired, the user can increase the value of N_K_3DCOR.

Additionally, independent codes were utilized to test the accuracy of halo mass function predictions. For the halo mass function, we compare the value of σ, $\log(\sigma^{-1})$, and the value of the halo mass function in the form used in Tinker et al. (2008),

$$\log[(M^2/\bar{\rho}_m)dn/dM]. \tag{69}$$

We note that while we maintain the 10^{-4} for our evaluations of σ, the accuracy degrades to a value of 5×10^{-3} for the halo mass function evaluation, primarily at the high halo mass and high redshift domains. We find that this increased error is acceptable, as the level of precision is significantly better than the accuracy of current halo mass function models.

4.3. *Validation of the power spectrum over parameter space*

Volunteer(s) in charge: Phil Bull

Suggested content: 'Fair' sampling of parameter space with Latin Hypercubes. Summary statistics used, and binning of power spectrum in k and z. Precision settings used for CLASS. Estimates of run-time. Results. Range of validity.

While concentrating on individual points in cosmological parameter space allows us to perform detailed validation tests, as above, it is important for CCL to also be validated across a wide range of cosmological parameter values, e.g. to ensure validity for MCMC analyses. In this section, we present a set of validation tests for the CCL linear and non-linear matter power spectrum functions that spans a broad rnage of ΛCDM parameters.

Covering a full range of all 5 ΛCDM parameters on a regular grid would be prohibitively expensive, so an alternative method for fairly (but more sparsely) sampling the parameter space is needed. We use Latin Hypercube Sampling to determine a tractably-sized set of sample points. This splits the parameter space into a regular grid with a given number of cells per dimension. The sample points are then chosen by going through each dimension in turn and choosing a cell at random *without replacement*, so that a given cell of a given dimension is only ever chosen once. This is repeated until all cells in all dimensions contain a single sample. This has the effect of covering the space uniformly but sparsely. The exact location of the sample within each cell can be chosen from a uniform distribution within that cell, but for simplicity we put each sample at the cell centre. The ranges used for each parameter are shown in Table 3.

Parameter	Range
h	$[0.5, 0.9]$
Ω_c	$[0.1, 0.4]$
Ω_b	$[0.018, 0.052]$
A_s	$[1.5 \times 10^{-9}, 2.5 \times 10^{-9}]$
n_s	$[0.93, 0.99]$

Table 3. Ranges of ΛCDM parameters used for the CCL validation tests.

For each set of parameters, we then calculate the linear and non-linear power spectra using CCL for a range of redshifts ($z \in \{0.0, 0.5, 1.0, 1.5, 2.0, 2.5\}$) and wavenumbers ($k \in [10^{-4}, 10^{0}]$ Mpc^{-1}). A corresponding set of reference power spectra is then produced using CLASS, which we run with settings chosen to produce high-precision results, taken from the pk_ref.pre precision file that is bundled with CLASS.

To quantify the level of agreement between the CCL and reference power spectra, we use the following summary statistic that can be summed over a chosen set of bins in redshift and wavenumber:

$$\Delta = \sum_{ij} \Theta \left(\log_{10} \left| \frac{P_{\rm CCL}(k_i, z_j) - P_{\rm ref}(k_i, z_j)}{P_{\rm ref}(k_i, z_j) \Delta_{\rm thres}} \right| \right). \tag{70}$$

Here, $\Delta_{\rm thres}$ is a target threshold for the fractional deviation between the power spectra, and we have defined $\Theta(x) \equiv x \;\; (x \geq 0)$ and 0 otherwise. Bins where the CCL power spectrum deviates from the reference power spectrum by a fraction less than $\Delta_{\rm thres}$ do not contribute to

the statistic, so the aim is to have $\Delta = 0$ (i.e. no deviation beyond the threshold in any bin). If deviations are found, however, they are weighted logarithmically – one large deviation of several orders of magnitude affects the statistic as much as a few smaller deviations of order $\sim \Delta_{\rm thres}$.

4.4. *Validation of the Cosmic Emulator*

Volunteer(s) in charge: Elisa Chisari

Lawrence et al. (2017) quantified the accuracy of the matter power spectrum from their emulation scheme by comparing their predictions to the resulting power spectra from the numerical simulations used for the calibration of their scheme. We repeated this procedure making the emulator predictions via `CCL` for a subset of emulator cosmologies. For cosmologies without neutrinos, we required the matter power spectrum at $z = 0$ to be within 1% of the smoothed simulated power spectrum from Lawrence et al. (2017) (see their Figure 6). Similarly, we required 3% accuracy for cosmologies with neutrinos (their Figure 5).

5. USAGE

Volunteer(s) in charge: Renee,Elisa

`CCL` is a public tool developed by the members of the Dark Energy Science Collaboration of LSST, and as such can be downloaded from the collaboration's github repository at the URL provided in the abstract. Installation instructions are provided in a README file available in that same repository. Instructions on how to generate a Docker[10] image are provided for portability to different architectures. `CCL` dependencies include the GNU Scientific Library[11] and FFTW3[12]. A suite of tests can be run to ensure installation was successful and all features perform nomrmally. Accuracy checks are performed in C, while a suite of unit tests is available in python.

`CCL` is documented using Doxygen[13]. For convenience, the repository includes multiple example files in C and several `Jupyter` notebooks.

`CCL` is released under terms consistent with BSD 3-Clause licensing.

6. OUTLOOK

Volunteer(s) in charge: David Alonso, Elisabeth Krause Science software development to facilitate the cosmological inference from LSST data is one of the critical task of the Dark Energy Science Collaboration (DESC). Recent cosmological analyses of the Dark Energy Survey (DES) relied on CosmoSIS (**?**) and CosmoLike (**?**), the Kilo-Degree Survey (KiDS) uses CosmoMC (**?**); all three frameworks employ CLASS, Camb, or the cosmic emulator to compute the density power spectra. Compared to the analyses of DES, KiDS and the Hyper-Suprime Cam Survey (HSC), future data sets (LSST, Euclid, WFIRST, etc) have substantially higher demands on analysis frameworks: The analyses are becoming more complex in terms of cosmological physics that is included in the analyses (neutrinos, modified gravity, and dark matter models) and in terms of modeling astrophysical and observational systematics at the required precision.

It is the primary goal of the `CCL` to become the backbone of all cosmological analyses carried out by the Dark Energy Science Collaboration of the LSST. This unified approach of a validated `CCL` will ensure that DESC results that are both consistent (in that they will all be based on the same theory framework) and accurate (in that this framework has undergone a rigorous numerical validation).

The implementation of `CCL` in realistic analysis pipelines has already begun: all likelihood module prototypes under development use it as its backbone, and the first of this, corresponding to the cosmological analysis of angular galaxy clustering cross-correlations, will serve as a model for the design of the joint-probes likelihood of the DESC DA:TJPCosmo-ers should feel free to strike this whole sentence out and rephrase as necessary!. This work has allowed us to validate the performance of `CCL` in a realistic analysis scenario, verifying its accuracy and efficiency in the context of computationally demanding MCMC runs. In addition to simulated analysis tests, `CCL` has also been validated through its use in the analysis of current datasets DA:I could include a couple of my papers here, but I don't know if we want to incur in self-citations. Do we know external papers that have used CCL?

Beyond its usefulness in the DESC, the generality of the design envisioned for `CCL` also aims to make it a useful tool for the analysis of other cosmological datasets, as well as for the cross-correlation of different experiments. To this end, and to allow a generic and flexible analysis of the LSST data, further functionality will be added to `CCL`. Plans are in place to extend the range of standard and non-standard cosmological models covered by the code. Work is already underway to add a comprehensive implementation of the halo-model calculation of two-point functions (Peacock & Smith 2000) with sufficient flexibility to include generic parametrizations of

[10] https://www.docker.com/
[11] https://www.gnu.org/software/gsl/
[12] http://www.fftw.org/
[13] www.doxygen.org/

observable halo profiles and mass-observable relations. The current simplified treatment of the galaxy-matter connection for galaxy clustering and intrinsic alignments will be improved by implementing generic perturbation-theory approaches to structure formation (McDonald & Roy 2009; McEwen et al. 2016b). A more complete implementation of all relevant cross-correlations between large-scale structure observables and other cosmological probes (e.g. CMB integrated Sachs-Wolfe effect (Sachs & Wolfe 1967) and other secondary anisotropies) will also soon be included.

In general, although this document presents the functionality and performance of `CCL` shortly after its release, we expect the library to be a continuously evolving piece of software. This will allow `CCL` to satisfy the analysis needs of future large datasets, as well as more accurate and sophisticated models for a broad range of cosmological and astrophysical observables.

ACKNOWLEDGMENTS

This paper has undergone internal review in the LSST Dark Energy Science Collaboration. **Thank the reviewers.**

The DESC acknowledges ongoing support from the Institut National de Physique Nucléaire et de Physique des Particules in France; the Science & Technology Facilities Council in the United Kingdom; and the Department of Energy, the National Science Foundation, and the LSST Corporation in the United States. DESC uses resources of the IN2P3 Computing Center (CC-IN2P3–Lyon/Villeurbanne - France) funded by the Centre National de la Recherche Scientifique; the National Energy Research Scientific Computing Center, a DOE Office of Science User Facility supported by the Office of Science of the U.S. Department of Energy under Contract No. DE-AC02-05CH11231; STFC DiRAC HPC Facilities, funded by UK BIS National E-infrastructure capital grants; and the UK particle physics grid, supported by the GridPP Collaboration. This work was performed in part under DOE Contract DE-AC02-76SF00515.

We would like to thank the organisers of the the DESC collaboration meetings at: Oxford (July 2016), SLAC (Ferurary 2018, March 2016), and ANL (2015), and the LSST-DESC Hack Week organisers (CMU, November 2016), where this work was partly developed. We would also like to acknowledge the contribution of the participants of the TJP Code Comparison Project, some of whom are among the `CCL` contributors, for providing the benchmarks for testing CCL. Finally, we are grateful for the feedback received from other working groups of DESC, including Strong Lensing, Supernovae and Photometric Redshifts.

And any acknowledgements you would like to add.

Author contributions are listed below.

Husni Almoubayyed: Reviewed code/contributed to issues.

David Alonso: Co-led project; developed structure for angular power spectra; implemented autotools; integrated into LSS pipeline; contributed to: background, power spectrum, mass function, documentation and benchmarks; reviewed code

Jonathan Blazek: Planning capabilities and structure; documentation and testing.

Philip Bull: Implemented the Python wrapper and wrote documentation for it; general bug fixes, maintenance, and code review; enhanced the installer and error handling system.

Jean-Éric Campagne: Angpow builder and contributed to the interface with CCL.

N. Elisa Chisari: Co-led project, coordinated hack projects & communication, contributed to: correlation function & power spectrum implementation, documentation, and comparisons with benchmarks.

Alex Drlica-Wagner: Helped with document preparation.

Zilong Du: Implemented the 3d correlation function.

Tim Eifler: Reviewed/tested code.

John Ellison: Implemented the 3d correlation function; documentation of 3d correlation function.

Renée Hlozek: Contributed initial code for error handling structures, reviewed other code edits.

Mustapha Ishak: Contributed to planning of code capabilities and structure; reviewed code; identified and fixed bugs.

Matthew Kirby: Performed comparison of physical constants.

David Kirkby: Writing, testing and reviewing code. Asking questions.

Elisabeth Krause: Initiated and co-led project; developed CLASS interface and error handling; contributed to other code; reviewed pull requests.

C. Danielle Leonard: Wrote and tested code for LSST specifications, user-defined photo-z interface, and support of neutrinos; reviewed other code; wrote text for this note.

Christiane S. Lorenz: Contributed to accurate high-redshift cosmological background quantities and benchmarked background splines.

Phil Marshall: Helped with document preparation.

Thomas McClintock: Wrote Python and doxygen documentation.

Sean McLaughlin: Wrote doxygen documentation and fixed bugs/added functionality to distances.

Jérémy Neveu: Contributed to Angpow and built the interface with CCL.
Stéphane Plaszczynski: Contributed to Angpow and contributed to the interface with CCL.
Javier Sanchez: Modified setup.py to allow pip installation and uninstall.
Sukhdeep Singh: Contributed to the correlation functions code.
Anže Slosar: Wrote and reviewed code.
Antonio Villarreal: Contributed to initial benchmarking, halo mass function code, and general code and issues review.
Michal Vrastil: Wrote documentation and example code, reviewed code.
Joe Zuntz: Wrote initial infrastructure, C testing setup, and reviewed code.

REFERENCES

Alonso, D., Bull, P., Ferreira, P. G., Maartens, R., & Santos, M. G. 2015, ApJ, 814, 145

Angulo, R. E., Springel, V., White, S. D. M., et al. 2012, MNRAS, 426, 2046

Bardeen, J. M., Bond, J. R., Kaiser, N., & Szalay, A. S. 1986, ApJ, 304, 15

Bartelmann, M., & Schneider, P. 2001, PhR, 340, 291

Blas, D., Lesgourgues, J., & Tram, T. 2011, CLASS: Cosmic Linear Anisotropy Solving System, Astrophysics Source Code Library, ascl:1106.020

Bonvin, C., & Durrer, R. 2011, PhRvD, 84, 063505

Campagne, J.-E., Neveu, J., & Plaszczynski, S. 2017, ArXiv e-prints, arXiv:1701.03592

Challinor, A., & Lewis, A. 2011, PhRvD, 84, 043516

Chevallier, M., & Polarski, D. 2001, International Journal of Modern Physics D, 10, 213

de Putter, R., & Takada, M. 2010, PhRvD, 82, 103522

Dodelson, S. 2004, Modern Cosmology, Vol. 57, 60–61, doi:10.1063/1.1784308

Durrer, R. 2008, The Cosmic Microwave Background (Cambridge University Press)

Eifler, T., Krause, E., Dodelson, S., et al. 2015, MNRAS, 454, 2451

Eisenstein, D. J., & Hu, W. 1998, ApJ, 496, 605

Hamilton, A. J. S. 2000, MNRAS, 312, 257

Hellwing, W. A., Schaller, M., Frenk, C. S., et al. 2016, MNRAS, 461, L11

Hirata, C. M., Mandelbaum, R., Ishak, M., et al. 2007, MNRAS, 381, 1197

Hirata, C. M., & Seljak, U. 2004, PhRvD, 70, 063526

Joachimi, B., & Bridle, S. L. 2010, A&A, 523, A1

Joachimi, B., Schneider, P., & Eifler, T. 2008, A&A, 477, 43

Kamionkowski, M., & Spergel, D. N. 1994, ApJ, 432, 7

Kilbinger, M., Heymans, C., Asgari, M., et al. 2017, ArXiv e-prints, arXiv:1702.05301

Kitching, T. D., Alsing, J., Heavens, A. F., et al. 2017, MNRAS, 469, 2737

Lattanzi, M., & Gerbino, M. 2017, ArXiv e-prints, arXiv:1712.07109

Lawrence, E., Heitmann, K., Kwan, J., et al. 2017, ApJ, 847, 50

Linder, E. V. 2003, Physical Review Letters, 90, 091301

McDonald, P., & Roy, A. 2009, JCAP, 8, 020

McEwen, J. E., Fang, X., Hirata, C. M., & Blazek, J. A. 2016a, JCAP, 9, 015

—. 2016b, JCAP, 9, 015

Mohammed, I., & Gnedin, N. Y. 2017, ArXiv e-prints, arXiv:1707.02332

Mohammed, I., & Seljak, U. 2014, MNRAS, 445, 3382

Ng, K.-W., & Liu, G.-C. 1999, International Journal of Modern Physics D, 8, 61

Ogata, H. 2005, Publications of the Research Institute for Mathematical Sciences, 41, 949

Peacock, J. A. 1999, Cosmological Physics, 704

Peacock, J. A., & Smith, R. E. 2000, MNRAS, 318, 1144

Sachs, R. K., & Wolfe, A. M. 1967, ApJ, 147, 73

Schneider, A., & Teyssier, R. 2015, JCAP, 12, 049

Semboloni, E., Hoekstra, H., & Schaye, J. 2013, MNRAS, 434, 148

Semboloni, E., Hoekstra, H., Schaye, J., van Daalen, M. P., & McCarthy, I. G. 2011, MNRAS, 417, 2020

Springel, V., Pakmor, R., Pillepich, A., et al. 2017, ArXiv e-prints, arXiv:1707.03397

Takahashi, R., Sato, M., Nishimichi, T., Taruya, A., & Oguri, M. 2012, ApJ, 761, 152

Talman, J. 2009, Computer Physics Communications, 180, 332

Tinker, J., Kravtsov, A. V., Klypin, A., et al. 2008, ApJ, 688, 709

Tinker, J. L., Robertson, B. E., Kravtsov, A. V., et al. 2010, ApJ, 724, 878

van Daalen, M. P., Schaye, J., Booth, C. M., & Dalla Vecchia, C. 2011, MNRAS, 415, 3649

Vogelsberger, M., Genel, S., Springel, V., et al. 2014, Nature, 509, 177

Watson, W. A., Iliev, I. T., D'Aloisio, A., et al. 2013, MNRAS, 433, 1230
Yoo, J. 2010, PhRvD, 82, 083508
Yoo, J., Fitzpatrick, A. L., & Zaldarriaga, M. 2009, PhRvD, 80, 083514